International Journal of Mechanical Sciences 163 (2019) 105115

Contents lists available at ScienceDirect

International Journal of Mechanical Sciences

journal homepage: www.elsevier.com/locate/ijmecsci

Design and numerical evaluation of recycled-carbon-fiber-reinforced polymer/metal hybrid engine cradle concepts

João Henrique Fonseca[a], Giyeol Han[a], Luca Quagliato[a], Yonghee Kim[a], Joeun Choi[a], Taeyeon Keum[b], Sungeun Kim[b], Do Suck Han[a], Naksoo Kim[a], Hyungyil Lee[a,*]

[a] Department of Mechanical Engineering, Sogang University, 35 Baekbeom-ro, Mapo-gu, Seoul 04107, Republic of Korea
[b] Research and Development Center, Donghee Industrial Company, Ulsan 44784, Republic of Korea

ARTICLE INFO

Keywords:
Multi-material design
Engine cradle
Recycled carbon fiber
Polymer-metal hybrid structures
Weight reduction

ABSTRACT

The design and evaluation of polymer-metal hybrid (PMH) engine cradles are realized via the design of concept models and finite element (FE) analyses. The structures consider a low-cost recycled carbon fiber (rCF) and PMH technologies. The initial conceptual design consists of creating C-type/hollow-type inserts and modifying the plastic components by considering the dimensions and thickness of insert and inclusion of plastic ribs as the design parameters. The PMH engine cradles are then evaluated by performance criteria, including weight reduction, stiffness, natural frequency and strength. The integration of rCF with injection-molding over metal inserts promoted weight reduction. The hollow-type and C-type PMH engine cradles achieved the weight reduction of 19 and 16% compared to the reference steel engine cradle, respectively, while they fulfilled the evaluation criteria. The results contribute to the advance of lightweight engine cradles with improved structural performance, fabricated with low-cost carbon fiber and fast manufacturing processes.

1. Introduction

The automotive industry has faced numerous challenges in the past decades regarding the emission of greenhouse gases from its automobiles. With the increasing awareness of global warming, especially in the last decade, governmental agencies have tightened regulations in order to bring CO_2 emissions to a minimum level. Weight reduction of vehicles have been achieved with lightweighting materials and computational optimization techniques [1–3]. Lightweighting improves the fuel efficiency up to 7% for each 10% reduction in vehicle weight [4].

Advanced materials emerged as important materials for automotive lightweighting, and they have been applied to numerous automotive parts, such as front ends, body structures and engine cradles [5]. The engine cradle (Fig. 1) is one of the key components of the engine subsystem and has as its main functions: (i) support the engine, transmission and suspension; (ii) distribute high chassis loads; (iii) reduce vibration and shocks; and (iv) contribute to rigidity and crash management. A regular engine cradle is commonly manufactured with welded steel stampings, having about 48 parts and 28 kg [6]. GM introduced the first all-wrought aluminum engine cradle in the 1999 Chevy Impala, weighing 18 kg with a total of 17 parts [6]. A thin-wall-casted magnesium engine cradle was first used on the Chevrolet Corvette Z06 from model year 2006 through 2013, in which weight was reduced to 10.5 kg with components integrated into a single-piece. Although polymers are expected to vastly compose newly developed vehicles, including electric ones [7], high costs of precursors and heat treatment [5,8–11] and long processing times [6] are the main barriers for a wider use of carbon-fiber-reinforced polymer (CFRP) composites in engine cradles and other automotive parts.

More recently, solutions like the use of rCF materials have been thought to overcome the high costs of CF materials [12–14]. The chassis component for the Zenos E10 sports car is an example of its recent commercial utilization. PMH manufacturing technologies allow to promote additional weight reduction by integrating metal and polymer materials in a single structure by means of faster-capability molding processes [15,16]. Such molding processes are efficient ways to produce polymer components [17] and process rCF into CFRP materials [18]. The PMH front-end of Audi A6, fabricated by injection overmolding, is the first reported case of the application of PMH technology into the automotive industry [19]. Thus, the integration of rCF materials and PMH technologies has the potential to reduce the total costs and manufacturing time to produce CFRP composite components.

Although several efforts have been made to achieve lightweighting of engine cradles through the replacement of steel by lightweighting materials, high cost, limited processing technology and incompatibility with existing infrastructure have restrained their further application

* Corresponding author.
E-mail address: hylee@sogang.ac.kr (H. Lee).

https://doi.org/10.1016/j.ijmecsci.2019.105115
Received 17 July 2019; Accepted 26 August 2019
Available online 31 August 2019

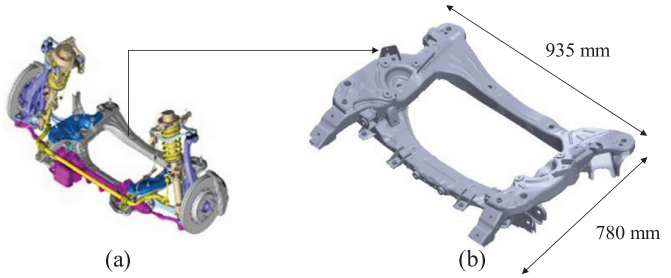

Fig. 1. Engine sub-system: (a) assembly of components (b) detail view of steel engine cradle.

[20]. Moreover, recent studies regarding the engine cradle have targeted the use of optimization techniques [21–23] and other traditional lightweight materials [24–26], while studies combining the capabilities of rCF and PMH technologies with engine subframes are scarce in the literature, or even inexistent. Thus, as any new material, rCF faces now major barriers that needs to be overcome, which are the lack of knowledge about mechanical properties, processing characteristics and large-scale demonstrators that prove the technical justification for its use [27].

Therefore, this study aims at developing multi-material engine cradles through the design of PMH concepts and investigating their structural performance through FE analyses. The design is carried out with focus on the conceptual design of the metal insert and CFRP components, where metal insert design, insert thickness, and inclusion of channels and ribs in the plastic component are the parameters considered. Weight reduction, stiffness, natural frequency and strength are set as the evaluation criteria. Furthermore, the resulting structural performance is analyzed and compared with the reference steel engine cradle (Fig. 1b).

2. Experimental procedure

To access the material properties of the 20% recycled-short-carbon fiber/polyamide (PA20%CF) that is the composite material considered in this study, injection-molded specimens were manufactured and three tensile tests performed according to the ASTM D–638. The tensile tests were carried out in an Instron machine at speed 2 mm/min. Fig. 2 shows the setup of the tensile experiment and the fractured specimen. The flow curves obtained in both experiments are shown in Fig. 3. The averaged mechanical properties obtained in the experiments can be seen in Table 1, where ρ is the density, E is the Young's modulus, ν is the Poisson's ratio, σ_y is the yield strength, and TS is the tensile strength. For simplification, anisotropic effects are not investigated and the material is considered isotropic with random distribution of fiber direction. The aluminum considered in this study is the AA 5083, widely employed by our industrial partner, Donghee Industrial Co. Ltd., in the automotive parts manufacturing. The mechanical properties were provided by the company, and it is also shown in Table 1.

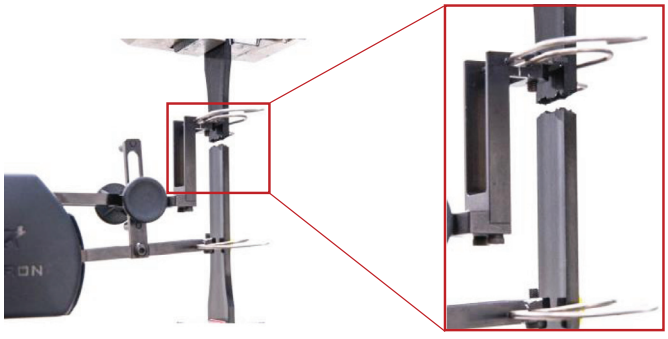

Fig. 2. Experiment setup and fractured PA20%CF specimen.

Table 1
Physico-mechanical properties of PA20%CF and AA 5083.

Material	ρ (kg/m^3)	E (GPa)	ν	σ_y (MPa)	TS (MPa)
PA20%CF	1160	15	0.42	157	210
AA 5083	2600	71	0.33	143	289

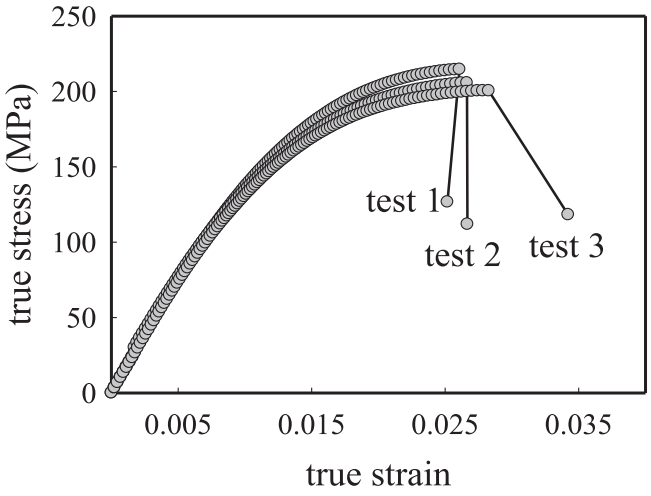

Fig. 3. Tensile test results of the PA20%CF specimens.

3. Design approaches

In the design process, the *conceptual* models are derived from an initial design volume (Fig. 4), which weights alone 23.9 kg when PA20%CF is considered and has the same width and length of the reference model. The main approach is to use aluminum insertions to deliver local stiffness and allow removal of CFRP material for weight reduction, which is the base material initially considered for the design volume. Two main ideas are considered for the insert: (i) a hollow-type and (ii) a C-type aluminum structure. A schematic illustration of both geometries in the PMH part can be seen in Fig. 5. Hereupon, a series of FE analyses are carried out to investigate the effects of insert thickness and addition of

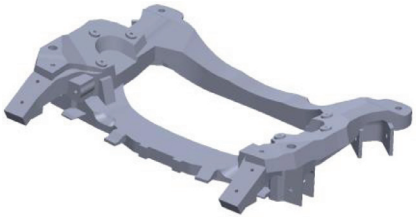

Fig. 4. Initial design domain.

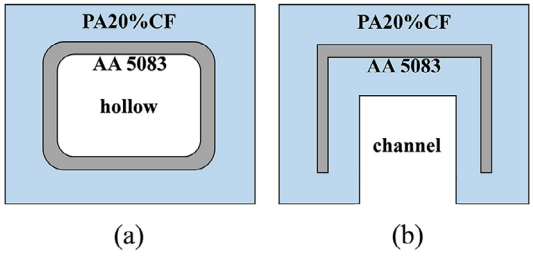

Fig. 5. Metal-insert approaches: (a) hollow-type (b) C-type.

plastic ribs. Finally, a detailed modeling is performed. In the conceptual design procedure, manufacturing restrictions, such as mold release and plastic thickness between insert and mold, are considered.

3.1. Hollow-type conceptual design procedure

The advantages of a hollow profile are to remove material in its most inner region and enable functional incorporation such as water channels and cable housing. Considering the hollow-type structure, to achieve weight reduction and preserve stiffness even after CFRP removal and aluminum insertion, it is necessary for the aluminum frame to occupy the same material volume that is being removed, and at the same time, provide enough stiffness. Considering the problem, there are three parameters to be modified to achieve the greatest weight reduction: (i) height h, (ii) width w, and (iii) thickness t of insert. To solve the problem, a search procedure is applied using the *Generalized Reduced Gradient* (GRG) nonlinear method [28], which allows nonlinear constraints and arbitrary bounds on the variables. It considers the gradient of the objective function P as the input values change and determines the optimum solution when the partial derivatives equal zero. Because the geometry of the initial design volume is relatively complex, the search procedure is conducted for a simple bar (Fig. 6) and the results approximated to the initial models. Here, the problem is to reduce the maximum weight by replacing PA20%CF by an AA 5083 tube. The objective function P used to maximize the ratio of the CFRP mass m_C removed by the aluminum mass m_S included is given by

$$P = \frac{m_C}{m_S} = \frac{h_C w_C}{\left[h_S w_S - (h_S - t)(w_S - t)\right]} \frac{\rho_C}{\rho_S} \tag{1}$$

where ρ_C and ρ_S are the material densities of PA20%CF and AA 5083, respectively. The ratio of deflection y under a fictional bending load, the ratio of torsion ϕ under a fictional torsional load, the local sectional dimensions of the initial design volume, and the allowed range of aluminum sheet thickness t are used as constraints, given by

$$y = \frac{E_C I_C}{E_S I_S} \leq 1 \Big\}; \quad \varphi = \frac{G_C I_C}{G_S I_S} \leq 1 \Big\}; \quad \begin{matrix} h_l \leq h \leq h_u \\ w_l \leq w \leq w_u \end{matrix} \Big\}; \quad 1.0 \leq t \leq 6\,\text{mm}\} \tag{2}$$

where E_C and E_S are the Young's modulus, G_C and G_S are the shear modulus, and I_C and I_S are the moment of inertia of the CFRP and aluminum bars, respectively. Additionally, h_l and h_u represent the lower and upper bounds of h, and w_l and w_u represent the lower and upper bounds of w, respectively. Finally, considering the allowed range of t, a total of eight constraints are created. The simple bar is locked in one end and the displacements are measured in the other end. The results showed that the greatest the dimensions h and w are, the greatest is the mass reduction achieved using the thickness t of 1.5 mm. Thus, the hollow-type insert is designed with a uniform thickness t of 1.5 mm and it considers a nominal wall thickness t_w (plastic thickness between insert and mold) of 5 mm from the outermost boundary and placed inside the CFRP component. Fig. 7 shows the plastic and metal structures. No ribs are considered in this concept model.

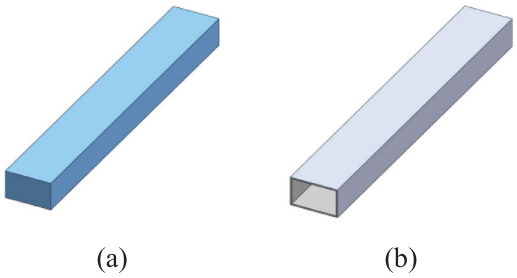

Fig. 6. Schematic representation of the simple bar used for the search procedure: (a) PA20%CF full section (b) AA 5083 tube.

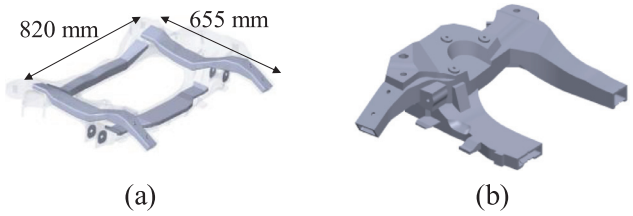

Fig. 7. Redesigned design volume with hollow-type approach: (a) aluminum insert (b) CFRP component (view cut).

3.2. C-type conceptual design procedure

Compared to a hollow-type structure, a C-type component has as its main advantage the simplification of manufacturing processes. The initial C-type PMH models are created based on FE simulations. In the C-type insert, a minimum t of 1.5 mm is considered, where the bottom part is removed to form a *C*-type design. In the CFRP component, plastic material is removed by creating channels following the metal structure with $t_w = 5$ mm and plastic ribs are included. Here, two types of structures are conceived: (i) basic C-type and (ii) C-type rib models; for the basic C-type structure, which consider no use of ribs, three models are created and the influence of t is investigated, which is applied as 1.5 (model C1), 2.0 (model C2), and 2.5 mm (model C3). Not to excessively increase the total weight, no thicker structures are considered; for the C-type rib structure, three models are created and the influence of plastic ribs and t is investigated. The models are C4, C5, and C6, which consider 1.5, 2.0, and 1.5 mm thick inserts, where in C6 extra ribs are included. For the creation of ribs, the following rules are followed

$$0.6\,t_w \leq t_r \leq t_w\}; \quad d_r \leq 7t_r\} \tag{3}$$

where t_r is the rib thickness and d_r is the rib depth. The ribs are placed in critical regions, such as in the rear cross member, middle section, and in the stabilizer bar area, where a considerable degree of torsion and bending are usually found. Fig. 8 shows the CFRP and aluminum structures.

3.3. FE modeling

The reference engine cradle (Fig. 1b) is composed of 44 steel stamped parts connected by means of seam weld and weights 22.2 kg. The

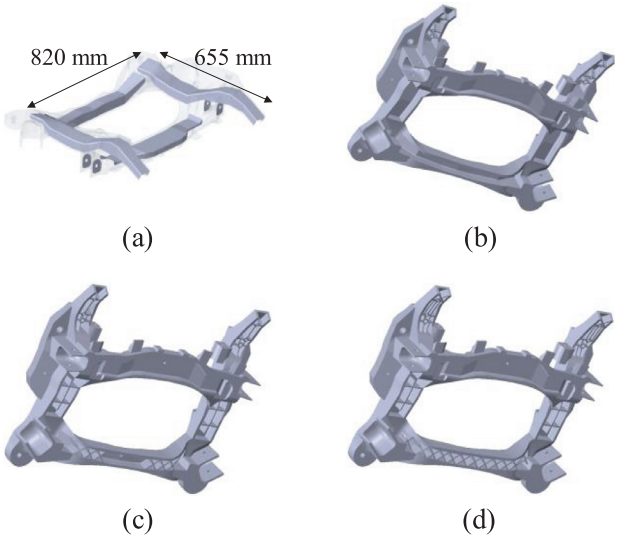

Fig. 8. Redesigned design volume with C-type approach: (a) aluminum insert and (b) basic (c) rib (d) extra rib CFRP components.

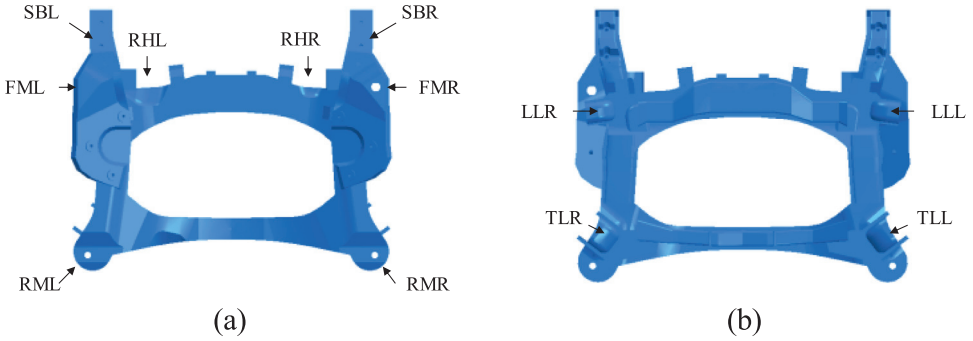

Fig. 9. Location of loading points: (a) top (b) bottom.

problem is simplified by considering all parts as shell structures and meshed with linear quadrilateral elements. Welds are considered as rigid elements. For the CFRP components, a solid section is assigned and meshed with quadrilateral tetrahedral elements while a shell section is applied to the inserts and meshed with linear quadrilateral elements. To simulate the connection between the plastic and metal, a *surface-to-surface*-type `TIE` constraint is employed, since it is somewhat more efficient and robust for complex surfaces [29]. The PA20%CF and AA 5083 material properties (Table 1) are applied to the CFRP and aluminum structures. The *lateral, longitudinal* and *vertical* loading conditions are considered. To distribute the loads in the structure, `MPC` and *kinematic coupling* constraints are created with `BEAM` elements. All loading points can be seen in Table 2, and their location is illustrated in Fig. 9.

Table 2
Loading points.

Loading point	ID	
	Left	Right
Front mount	FML	FMR
Rear mount	RML	RMR
Lateral link	LLL	LLR
Tension link	TLL	TLR
Rack housing	RHL	RHR
Stabilizer bar	SBL	SBR

3.4. Mass and strain energy of initial PMH models

FE analyses were carried out for every model and the results are shown in Fig. 10, where strain energy was set to control the overall stiffness of the models. Under *lateral* and *longitudinal* loadings, the strain energy is much lower than for the reference value, indicating great stiffness of the designs, especially for the C-type rib and hollow models. Under *vertical* loading, the C-type rib and hollow models present a slight lower strain energy than the reference value. However, the strain energy gets much higher for the basic C-type models, indicating that the models are less stiff in this case. Despite that stiffness improves in all

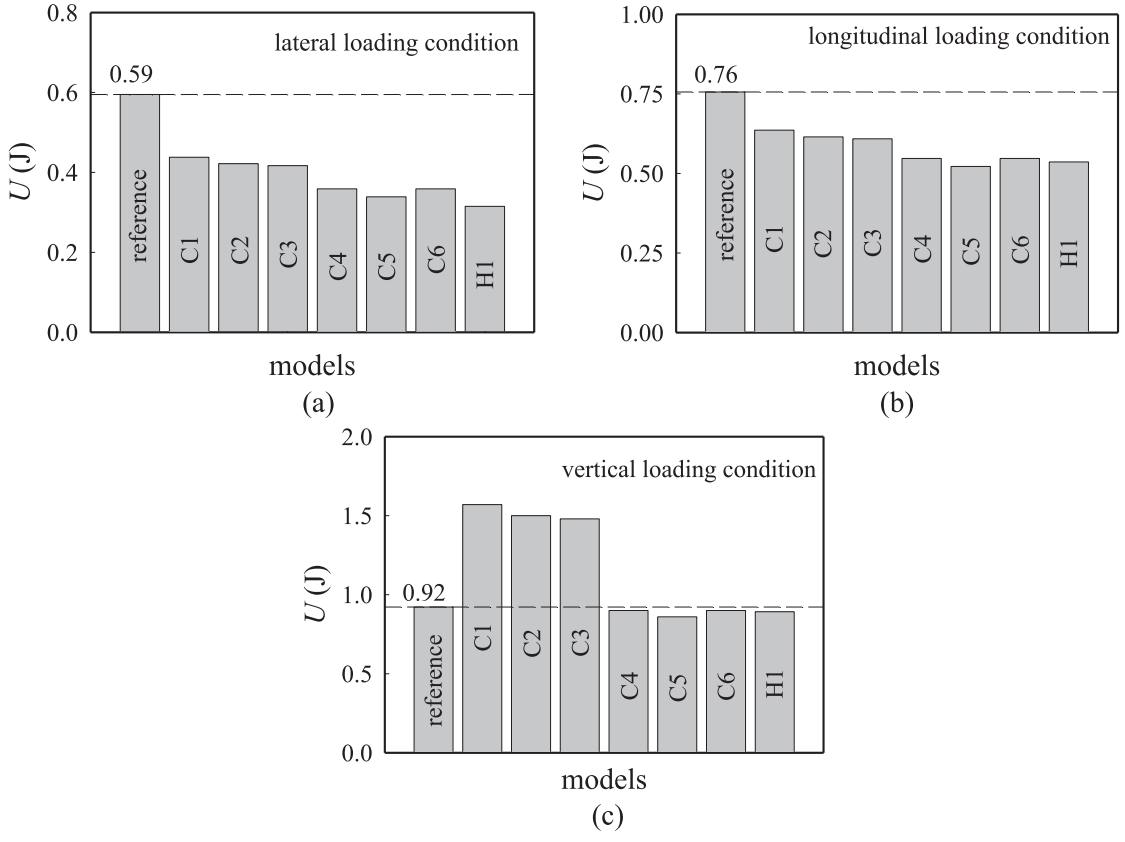

Fig. 10. Strain energy of the initial PMH engine cradles under: (a) *lateral* (b) *longitudinal* (c) *vertical* loading conditions.

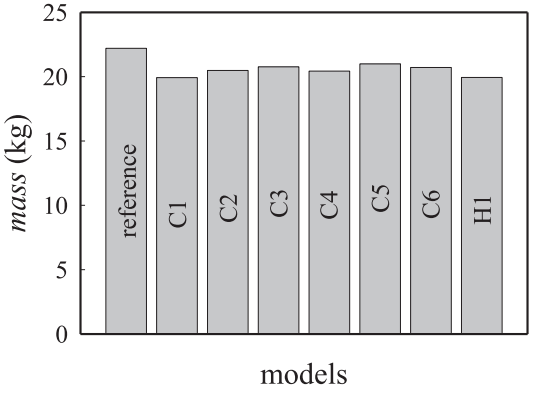

Fig. 11. Total mass of the reference and initial PMH engine cradles.

loading conditions when thickness is increased, it is still inferior under the *vertical* condition. Hence, the models without ribs are not considered in the detailed design phase. Moreover, the results show that when extra ribs are included (C6), stiffness shows almost no improvements. However, when thickness is increased to 2.0 mm (C5), the strain energy is reduced in all loading conditions. This shows that once the basic ribs are included, insert thickness has greater influence on stiffness. Since the stiffness of C4 and C5 are fairly similar, model C4 is selected as the optimal C-type model, yielding the greatest weight reduction of 8.0% (Fig. 11). Finally, H1 presented greater stiffness in almost all cases with the greatest weight reduction of 10.2%.

3.5. Detailed design process

After the development of different PMH models, C4 and H1 yielded the greatest results, and thus, they were selected to compose the detailed design stage. The goals of this step are: (i) address basic design/manufacturing considerations and (ii) obtain further weight reduction. In the design of any component, it is crucial to consider the manufacturing process by which the parts are made. Because the PMH models are considered to be manufactured by injection overmolding, a few parameters are important to be considered in this case, such as wall thickness, corners, rib dimensions and draft angle. Thus, in addition to Eq. (3), the models are modified according to the guideline

$$0.6t_w \le r_{in} \le t_w\}; \quad r_{out} = r_{in} + t_w\}; \quad \alpha \ge 1.5°\}. \tag{4}$$

where r_{in} is the internal radius, r_{out} is the external radius, and α is the draft angle, avoiding sharp increase in stress concentrations at low ratio of radius to wall thickness ($r_{in}/t_w \le 0.4$) and allowing the part to be ejected from the mold. Moreover, thick sections are also an issue for plastic-injected parts. The main problems usually encountered are long cooling times and shrinkage, generating sink marks, voids, and distortion. Thus, C4 and H1 are modified according to Eqs. (3) and (4), transforming the remaining solid shapes in shell-like forms, allowing for further weight reduction. The detailed hollow (detailed-H) and C-type (detailed-C) models can be seen in Fig. 12, yielding a weight reduction of 19% and 16%, respectively (Fig. 13).

4. Results and discussion

4.1. Stiffness

After the detailed design and further weight reduction, new FE analyses were performed. The stiffness-related results (Fig. 14) show an overall similar stiffness of the detailed models and the reference model. Under the *lateral* loading, the strain energy of the PMH models is considerably lower than the reference values. Under the *longitudinal* loading, the strain energy is slightly lower for the PMH models. This loading condition was the most affected by the detailed design stage in terms

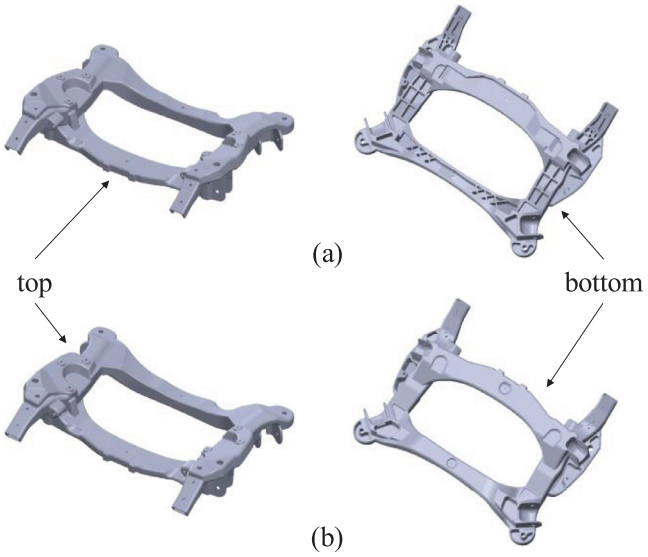

Fig. 12. Detailed PMH models: (a) detailed-C (b) detailed-H.

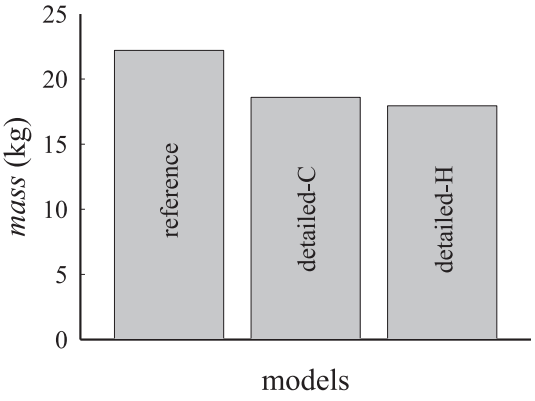

Fig. 13. Total mass of the reference and detailed PMH engine cradles.

of stiffness. Under the *vertical* loading, the strain energy of detailed-C is same with the reference value and lower for detailed-H. Almost no variation in strain energy was found in this case, since material was not removed in its most critical area (stabilizer bar). Additionally, the removal of sharp edges by including fillets helped to keep the strain energy inside the admissible range. The displacement magnitude of detailed-H is similar with the reference model, while it is slightly higher for detailed-C, which shows a higher flexibility than all other models. Moreover, the rear zone seems to be the most critical area. Finally, detailed-H is shown to be more efficient in terms of structural performance. These results show that PMH engine cradles can provide stiff solutions and lighter designs than the regular steel design.

4.2. Natural frequency

By considering a vehicle with a four-cylinder, four stroke engine, the fundamental excitation frequency of vibration is according the harmonic of the second order with respect to engine rotational speed [30]. Thus, in this case, the excitation frequency lays in the range 20–200 Hz for an engine rotational speed in the 600–6000 rpm range, meaning that the engine cradle's natural frequency should be greater than 200 Hz. To obtain the eigenvalues and calculate the natural frequencies, *subspace iteration* [29] is applied. The first six natural frequencies are extracted (Fig. 15), where the first is a flexural vibration mode. The first natural frequency of the reference engine cradle is 165 Hz, indicating that

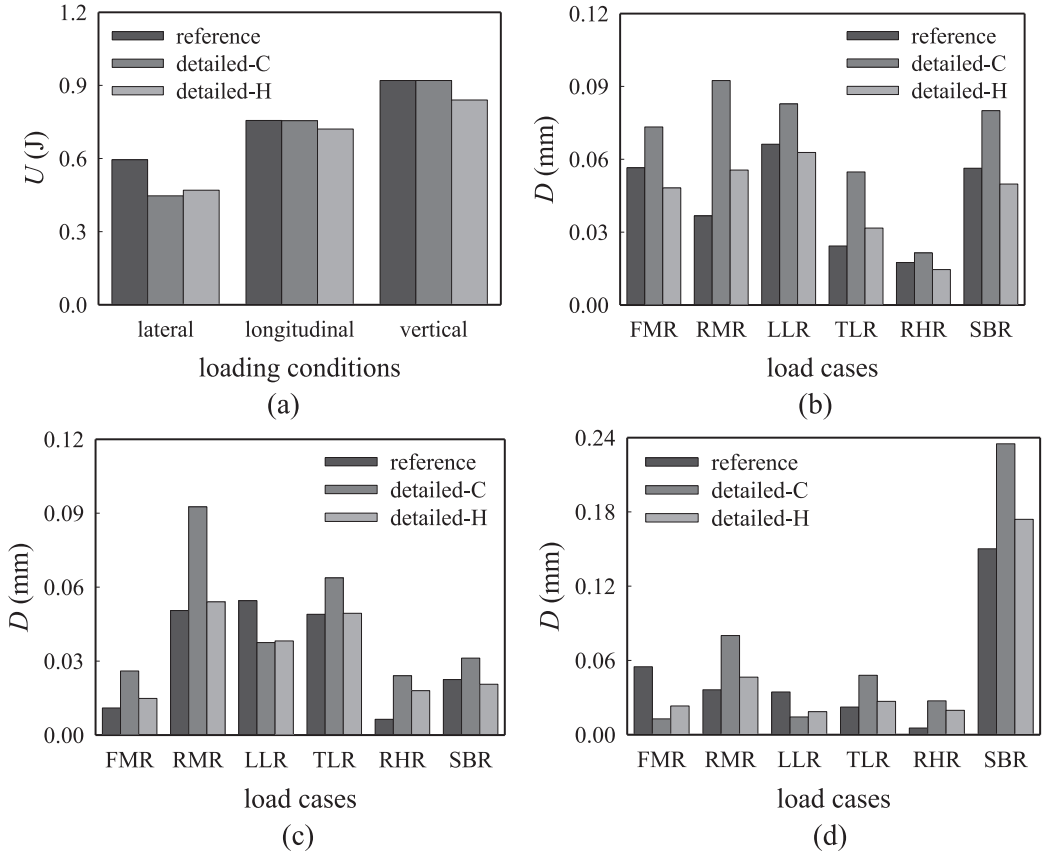

Fig. 14. Stiffness-related results of the detailed PMH models: (a) strain energy and (b) *lateral* (c) *longitudinal* (d) *vertical* loading conditions displacement magnitude values.

this design may not be optimal in terms of vibration isolation at high rotational speeds. For the detailed-C and detailed-H, the first natural frequency is 214 Hz and 255 Hz, respectively. Therefore, the PMH models showed improved behavior in terms of vibration isolation, which can also be attributed to the use of polymers that are known to reduce vehicle noises and vibrations [31–33].

4.3. Strength analysis

In the strength analysis, six *heavy static loads* are applied to the structures with different intensities (Table 3). The goal is to determine whether it can endure the loading conditions without reaching the ultimate static failure, in which case the structure is considered a good candidate as a lightweight engine cradle. Table 3 summarizes the results. In most of the loading conditions, the inserts show some degree of plastic deformation. However, the strain is kept much lower than the strain at failure of the material. For the CFRP components, the strains are mostly in the elastic range. However, the back and inward loadings are the most severe cases, where a considerably large plastic deformation was found for both structure types. Nonetheless, the strains are kept lower than the strain at failure of PA20%CF, indicating that no static failure takes place. Both the detailed-H and detailed-C models provided good results in the strength evaluation phase with similar results, where detailed-H presented lower strains for the insert component while detailed-C presented lower strains for the CFRP component.

Table 3
Summary of strength analysis results.

Load type	Intensity (G)	Component	detailed-C		detailed-H	
			Maximum principal strain (10^{-3})	Condition	Maximum principal strain (10^{-3})	Condition
Backward	6	PA20%CF	7.3	No failure	9.9	No failure
		AA 5083	3.5	No failure	1.9	No failure
Forward	2	PA20%CF	2.4	No failure	2.5	No failure
		AA 5083	0.9	No failure	0.6	No failure
Inward	6	PA20%CF	19.2	No failure	24.1	No failure
		AA 5083	10.0	No failure	6.4	No failure
Outward	2	PA20%CF	3.2	No failure	4.4	No failure
		AA 5083	1.6	No failure	1.1	No failure
Upward	7	PA20%CF	5.1	No failure	9.1	No failure
		AA 5083	7.1	No failure	2.1	No failure
Downward	2	PA20%CF	5.1	No failure	9.6	No failure
		AA 5083	7.5	No failure	2.3	No failure

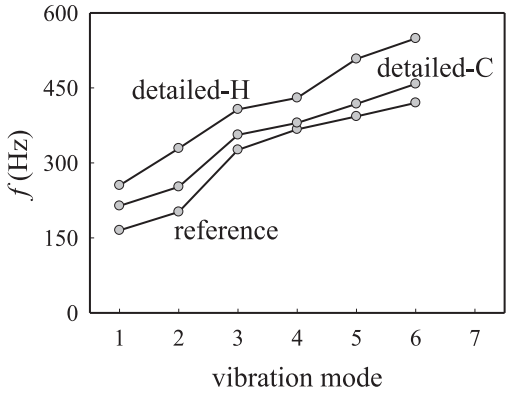

Fig. 15. Natural frequency for the first 6 vibration modes of reference, detailed-C and detailed-H models.

5. Conclusion

This study demonstrated the feasibility of considering polymer-metal hybrid engine cradles for weight reduction and enhancement of structural performance by integrating a rCF material and PMH technologies that allow reducing process-time of CFRP components. The steps related to the initial design of a PMH engine cradle, including metal insert and CFRP components design, are thoroughly explored. This work serves as a guideline to the future development of PMH engine cradles, and it can be applied for other structural components. A C-type and a hollow-type PMH engine cradles were conceived. Both structures were shown to be able to meet the evaluation criteria, including the total weight reduction, stiffness, natural frequency, and strength. The hollow-type structure obtained the best results in terms of structural performance with 19% weight reduction in relation to the reference model. The C-type model showed superior results compared to the reference model with 16% weight reduction and a possible lower manufacturing cost than the hollow-type structure. The results add to the development of a new generation of lightweight automotive components with capability of being produced on the large-scale manufacturing. Ongoing research topics include: (i) PMH engine cradle design via advanced design optimization techniques; and (ii) manufacturing analysis of PMH engine cradles by insert injection molding.

Acknowledgement

This work was supported by the Carbon Industrial Cluster Development Program (No. 10083609) funded by the Ministry of Trade, Industry & Energy (MOTIE, Korea).

References

[1] Bolar N, Buchler T, Li A, Wallace J. MMLV: vehicle durability design, simulation and testing. SAE Tech Pap Ser 2015;1. doi:10.4271/2015-01-1613.
[2] Kastensson Å. Developing lightweight concepts in the automotive industry: taking on the environmental challenge with the Sånätt project. J Clean Prod 2014;66:337–46. doi:10.1016/j.jclepro.2013.11.007.
[3] Zhang Y, Zhu P, Chen G. Lightweight design of automotive front side rail based on robust optimisation. Thin-Walled Struct 2007;45:670–6. doi:10.1016/j.tws.2007.05.007.
[4] Joost WJ. Reducing vehicle weight and improving U.S. energy efficiency using integrated computational materials engineering. Jom 2012;64:1032–8. doi:10.1007/s11837-012-0424-z.
[5] Taub AI, Luo AA. Advanced lightweight materials and manufacturing processes for automotive applications. MRS Bull 2015;40:1045–54. doi:10.1557/mrs.2015.268.
[6] Taub AI, Krajewski PE, Luo AA, Owens JN. Yesterday, today and tomorrow: the evolution of technology for materials processing over the last 50 years: the automotive example. JOM 2007. doi:10.1007/s11837-007-0022-7.
[7] Lyu MY, Choi TG. Research trends in polymer materials for use in lightweight vehicles. Int J Precis Eng Manuf 2015;16:213–20. doi:10.1007/s12541-015-0029-x.
[8] Dong X, Lu C, Zhou P, Zhang S, Wang L, Li D. Polyacrylonitrile/lignin sulfonate blend fiber for low-cost carbon fiber. RSC Adv 2015. doi:10.1039/c5ra01241d.
[9] Baker DA, Gallego NC, Baker FS. On the characterization and spinning of an organic-purified lignin toward the manufacture of low-cost carbon fiber. J Appl Polym Sci 2012. doi:10.1002/app.33596.
[10] Braun JL, Holtman KM, Kadla JF. Lignin-based carbon fibers: oxidative thermostabilization of kraft lignin. Carbon N Y 2005. doi:10.1016/j.carbon.2004.09.027.
[11] Kadla JF, Kubo S, Venditti RA, Gilbert RD, Compere AL, Griffith W. Lignin-based carbon fibers for composite fiber applications. Carbon N Y 2002. doi:10.1016/S0008-6223(02)00248-8.
[12] Holmes M. Recycled carbon fiber composites become a reality. Reinf Plast 2018;62:148–53. doi:10.1016/j.repl.2017.11.012.
[13] Meng F, McKechnie J, Turner T, Wong KH, Pickering SJ. Environmental aspects of use of recycled carbon fiber composites in automotive applications. Environ Sci Technol 2017;51:12727–36. doi:10.1021/acs.est.7b04069.
[14] Oliveux G, Dandy LO, Leeke GA. Current status of recycling of fibre reinforced polymers: review of technologies, reuse and resulting properties. Prog Mater Sci 2015;72:61–99. doi:10.1016/j.pmatsci.2015.01.004.
[15] Grujicic M. Injection overmolding of polymer-metal hybrid structures. In: Amancio–Filho ST, Blaga L-A, editors. Join Polym Hybrid Struct Princ Appl. Hoboken: Wiley; 2018. p. 277–305.
[16] Carradò A, Faerber J, Niemeyer S, Ziegmann G, Palkowski H. Metal/polymer/metal hybrid systems: towards potential formability applications. Compos Struct 2011. doi:10.1016/j.compstruct.2010.07.016.
[17] Park HS, Dang XP, Roderburg A, Nau B. Development of plastic front side panels for green cars. CIRP J Manuf Sci Technol 2013;6:44–52. doi:10.1016/j.cirpj.2012.08.002.
[18] Wong KH, Syed Mohammed D, Pickering SJ, Brooks R. Effect of coupling agents on reinforcing potential of recycled carbon fibre for polypropylene composite. Compos Sci Technol 2012. doi:10.1016/j.compscitech.2012.02.013.
[19] Korson C, Stratton D. An integrated automotive roof module concept: platic-metal hybrid and polyurethane composite technology. In: Proc. 5th SPE Annu. Automot. Compos. Conf.; 2005. p. 14–15.
[20] Joost WJ, Krajewski PE. Towards magnesium alloys for high-volume automotive applications. Scr Mater 2017;128:107–12. doi:10.1016/j.scriptamat.2016.07.035.
[21] Li C, Kim IY. Multi-material topology optimization for automotive design problems. Proc Inst Mech Eng Part D J Automob Eng; 2018. doi:10.1177/0954407017737901.
[22] Lim W, Jang J, Kim S, Lee TH, Kim J, Lee K, et al. Reliability-based design optimization of an automotive structure using a variable uncertainty. Proc Inst Mech Eng Part D J Automob Eng 2016;230:1314–23. doi:10.1177/0954407015606825.
[23] Li C, Kim IY, Jeswiet J. Conceptual and detailed design of an automotive engine cradle by using topology, shape, and size optimization. Struct Multidiscip Optim 2015;51:547–64. doi:10.1007/s00158-014-1151-6.
[24] Doude H, Oglesby D, Gullett PM, Kadiri H El, Jelinek B, Baskes MI, et al. Cast magnesium alloy corvette engine cradle. In: Horstmeyer MF, editor. Integr. Comput. Mater. Eng. Met. Concepts Case Stud.. Hoboken: Wiley; 2018. p. 337–76.
[25] Belingardi G, Koricho EG. Design of a composite engine support sub-frame to achieve lightweight vehicles. Int J Automot Compos 2014;1:90. doi:10.1504/ijautoc.2014.064129.
[26] Pinch W, Aragones J, Osborne R, Kolp S, Ouimet L, Goundan K. Development of the 2006 corvette Z06 structural cast magnesium crossmember. SAE Tech Pap Ser 2010. doi:10.4271/2005-01-0340.
[27] Holmes M. Lowering the cost of carbon fiber. Reinf Plast 2017;61:279–83. doi:10.1016/j.repl.2017.02.001.
[28] Lasdon LS, Fox RL, Ratner MW. Nonlinear optimization using the generalized reduced gradient method. Rev Française d'automatique, Informatique, Rech Opérationnelle Rech Opérationnelle 1974;8:73–103. doi:10.1051/ro/197408v300731.
[29] Abaqus Version 6.14. User's Manual 2014.
[30] Yu Y, Naganathan NG, Dukkipati RV. Literature review of automotive vehicle engine mounting systems. Mech Mach Theory 2001. doi:10.1016/S0094-114X(00)00023-9.
[31] Demirci MT, Düzcükoğlu H. Wear behaviors of polytetrafluoroethylene and glass fiber reinforced polyamide 66 journal bearings. Mater Des 2014. doi:10.1016/j.matdes.2014.01.013.
[32] Ünlü BS, Atik E, Köksal S. Tribological properties of polymer-based journal bearings. Mater Des 2009. doi:10.1016/j.matdes.2008.11.018.
[33] Chang L, Zhang Z, Zhang H, Schlarb AK. On the sliding wear of nanoparticle filled polyamide 66 composites. Compos Sci Technol 2006. doi:10.1016/j.compscitech.2005.02.021.